Double Drug-Loaded and pH/Thermal Sensitive Multifunctional Drug Delivery System for Tumor Photoacoustic Imaging-Guided Enhanced Chemo/Photothermal Therapy

Jun Wang
Tongji University
Na Chen
Soochow University
Kai Liu
Tongji University
Yu Tu
Soochow University
Weitao Yang
Tongji University
Xiaolong Gao
BaoshanBranch of Fudan University
Weiwei Zeng
Tongji University
Bingbo Zhang (bingbozhang@tongji.edu.cn)
Tongji University https://orcid.org/0000-0002-0981-7071

Research

Keywords: Mesoporous silica, Gold nanorods, Chemo/photothermal therapy, Drug release, Photoacoustic imaging

Posted Date: December 30th, 2019

DOI: https://doi.org/10.21203/rs.2.19618/v1

Abstract

Background: Owing to the tunability of longitudinal surface plasmon resonance (LSPR), ease of synthesizing small size and excellent stability, AuNRs have been developed as photothermal agents for cancer therapy. However, PTT alone could not kill cancer cells completely due to the local heterogeneous distribution of heat in tumors, penetration depth of light, light scattering and absorption. In addition, the treatment systems based on AuNRs hold disadvantages of loading one antitumor drug or a low therapeutic efficiency. Therefore, the construction of the AuNRs theranostic system to achieve imaging-guided dual drug delivery and enhanced photothermal therapy for tumor still remains a great challenge.

Methods: The AuNRs were prepared using a seedless method. A mesoporous silica shell layer was coated on the surface of the AuNRs by sol-gel method. Double anticancer drugs, DOX and Btz, were loaded into the AuNRs@MSN nanoparticles through physical absorption and covalent conjugation, respectively.

Results: The release of DOX and Btz is found pH/thermal dual responsive in vitro. Compared with AuNRs@MSN, PDA-AuNRs@MSN exhibits an increased near-infrared (NIR) absorption at 808 nm and an enhanced photothermal effect. In contrast to chemotherapy or photothermal therapy alone, the integrated D/B-PDA-AuNRs@MSN nanoparticles show higher cell apoptosis and enhanced tumor treatment efficacy *in vitro* and *in vivo*.

Conclusions: In this study, we designed a double-drug loading, enhanced chemo/photothermal therapy and pH/thermal responsive drug delivery system for photoacoustic (PA) imaging-guided tumor therapy. We believe that the multifunctional D/B-PDA-AuNRs@MSN theranostic probe could serve as an effective probe for the treatment of cancers.

Background

Cancer is one of the greatest threats to human health [1]. At present, the most common ways for cancer treatment are chemotherapy, surgery and radiotherapy in clinical. However, these approaches usually result in adverse side effects. Recently, the near-infrared (NIR) light-driven nanomaterials-mediated photothermal therapy (PTT) has attracted extensive attention due to its advantages of being non-invasive and few side effects. The mechanism of the PTT is based on the principle that the photothermal agents absorb the NIR light converting into heat, leading to cancer cell ablation and death [2]. In this regard, gold nanomaterials, such as gold nanostructure (gold nanoparticles (AuNPs) [3-5], gold nanorods (AuNRs) [6-9], gold nanocages (AuNCs) [10-12], gold nanostars [13-15], gold nanoshell [16-18] and gold nanoflowers [19]) have been developed as photothermal agents for cancer therapy.

Among these gold nanomaterials, AuNRs have been widely used in the field of biomedicine due to the tunability of longitudinal surface plasmon resonance (LSPR), ease of synthesizing small size and excellent stability. However, PTT alone could not kill cancer cells completely due to the local heterogeneous distribution of heat in tumors, light scattering and absorption [20]. In addition, the energy of the light was gradually decreased with the depth of penetration into the tissues [21]. Compared with

single therapy, combination therapy, such as chemo-photothermal therapy, is considered as an effective strategy to enhance therapeutic efficiency because this strategy has the advantages of reducing the negative effects and overcoming the drug resistance of tumor cells. However, the treatment systems based on AuNRs hold disadvantages of loading one antitumor drug or a low therapeutic efficiency [22, 23]. Therefore, the construction of the AuNRs theranostic system to achieve imaging-guided control over dual drug delivery and enhanced photothermal therapy for tumor still remains a great challenge.

In this study, we developed a double-drug loading and pH/thermal dual sensitive drug delivery system for imaging-guided multi-modal cancer therapy based on polydopamine-coated mesoporous silica-AuNRs. In this drug delivery system, nanoscale mesoporous silica-coated AuNRs encapsulating doxorubicin hydrochloric acid (DOX) was designed as a core. Polydopamine (PDA) was deposited on the surface of the mesoporous silica@AuNRs by oxidative self-polymerization for enhanced PTT and controlled drug release as gatekeepers. Another anti-tumor drug bortezomib (Btz) was combined to PDA through boronic acid of Btz and catechol of PDA conjugation. The resulting multifunctional nanocarriers possess the properties of enhanced chemo-photothermal therapy and pH/thermal-responsive controlled drug release.

Methods

Materials

Tetraethylorthosilicate (TEOS, 99%) was purchased from Sigma-Aldrich. Cetyltrimethylammonium bromide (CTAB), ascorbic acid (AA)、ethanol and hydrochloric acid were acquired from Sinopharm Chemical Reagent Co., Ltd. Sodium borohydride ($NaBH_4$), 4, 6-diamidino-2-phenylindole (DAPI) and sodium hydroxide were purchased from Aladdin (Shanghai, China). Silver nitrate ($AgNO_3$) and Dopamine hydrochloride were purchased from Alfa Aesar. Tetrachloroauric acid ($HAuCl_4 \cdot 3H_2O$) was purchased from Huawei Chemical Reagent Co., Ltd. Doxorubicin hydrochloride (DOX·HCl, 98%) and bortezomib were obtained from Dalian Meloney Biotechnology Co., Ltd (Dalian, China). China). Millipore water with 18.2 MΩ was used in the experiment.

Synthesis of AuNRs

The AuNRs were prepared using a seedless method with slight modifications [24, 25]. Briefly, CTAB solution (30 mL, 0.2 M) was added to 30 mL of 1.0 mM $HAuCl_4$, followed by the addition of 1.8 mL of 4 mM $AgNO_3$ and 72 μL of HCl (37%). Next, 450 μL of 85.8 mM AA was added and gently swirled as the solution became colorless. Finally, 45 μL of 10 mM $NaBH_4$ was rapidly injected. The resulting solution was kept for 6 h at 30 °C.

Preparation of AuNRs with mesoporous silica shell (AuNRs@MSN)

AuNRs@MSN were synthesized according to the reported previously [26]. To remove excess CTAB from AuNRs, 30 mL of the as-synthesized AuNRs was centrifuged at 16 000 rpm for 30 minutes. The precipitate was redispersed in 30 mL of Milli-Q water and 300 μL of 0.1 M NaOH solution was added

upon stirring. Then, three injections of 90 μL of 20% TEOS in methanol solution was added into the above solution at 30 minutes intervals. The mixture was stirred for 24 h at 30 °C. The AuNRs@MSN were separated by centrifugation. The precipitate was refluxed with 20 mL of 10 mg/mL NH_4NO_3-ethanol solution under 60 °C for 12 h to extract the surfactant template CTAB. The final product was collected by centrifugation at 16 000 rpm for 30 min and washed with ethanol three times. The as-synthesized solid was dried in the lyophilizer.

Synthesis of PDA coated DOX-AuNRs@MSN (PDA-DOX-AuNRs@MSN)

The PDA-DOX-AuNRs@MSN were synthesized according to the literatures [27, 28]. AuNRs@MSN (50 mg) was added to the DOX solution (1 mg/mL, 5 mL) and stirred in dark at the room temperature for 24 h. The product was acquired by centrifugation and washed with deionized water until the supernatant became colorless. The DOX-AuNRs@MSN (50 mg) nanoparticles were suspended in the 50 mL of Tris-HCl buffer solution (pH 8.5, 10 mM). Then dopamine hydrochloride (25 mg) was added and stirred in dark at room temperature for 24 h. The PDA-DOX-AuNRs@MSN were collected by centrifugation and washed with deionized water several times to remove the unpolymerized dopamine. PDA-AuNRs@MSN were synthesized according to the same procedure without adding the DOX. The loading efficiency (LE%) of DOX on AuNRs@MSN was calculated using the following formula: LE% = $(M_{DOX1}-M_{DOX2})/M_{DOX1}$, where M_{DOX1} is the added DOX content and M_{DOX2} is the supernatant DOX content.

Synthesis of DOX/Btz-PDA-AuNRs@MSN (D/B-PDA-AuNRs@MSN)

Btz were conjugated to the PDA-DOX-AuNRs@MSN according to the reported literatures [29, 30]. The PDA-DOX-AuNRs@MSN were dispersed in 10 mL of dimethylsulfoxide (DMSO)-deionized water (1:10, v/v) solution containing 5 mg of Btz. The mixture was stirred for 24 h at room temperature. The products were separated by centrifugation and washed with deionized water. The loading efficiency (LE%) of Btz on DOX-PDA-AuNRs@MSN was calculated using the following formula: LE% = $(M_{Btz1}-M_{Btz\ 2})/M_{Btz1}$, where M_{Btz1} is the added Btz content and M_{Btz2} is the supernatant Btz content.

In vitro drug release

D/B-PDA-AuNRs@MSN were dispersed in 2 mL of buffer solutions (pH 5.0 and 7.4), respectively. The dispersion solution was then transferred into a dialysis bag (molecular weight cut off =8 000-14 000 kDa) and placed in 100 mL of PBS buffer solution at 37 °C with or without 808 nm light irradiation and shaked at 150 rpm. At timed intervals, 3 mL of solution was withdrawn from the solution. The released DOX and Btz were analyzed by UV-vis spectrum. The volume of the release medium was kept constant by adding 3 mL fresh medium after each sampling.

In vitro cytotoxicity

The cell viability was determined by CCK-8 assay. 4T1 cells were seeded into a 96-well plate at a density of 1×10^4 cells and cultured at 5% CO_2 and 37 °C for 24 h. Different concentrations of AuNRs@MSN,

PDA-AuNRs@MSN, free DOX+Btz, D/B-PDA-AuNRs@MSN were added to the medium, and the cells were incubated at 5% CO_2 and 37 °C for 24 h. In order to evaluate PTT efficacy, PBS, AuNRs@MSN, PDA-AuNRs@MSN, D/B-PDA-AuNRs@MSN were cultured with 12 h before the cells were irradiated with 808 nm laser (1 W/cm^2) for 5 min. The cells were further incubated for another 12 h. The cell viability was calculated by measuring the absorbance value at 450 nm.

In vitro cellular uptake

4T1 cells were seeded into confocal dish and cultured for 24 h. The D/B-PDA-AuNRs@MSN solution (DOX concentration = 2 μg/mL, Btz concentration = 0.1 μg/mL) was added and cultured with cells for 4 h. Then, the cells were washed with PBS solution and fixed with 4% formaldehyde for 10 min. After that, the cells were washed with PBS solution several times to remove excess formaldehyde. The cell nuclei was stained by DAPI. The fluorescence images were observed under confocal laser scanning microscopy (CLSM).

Temperature measurement *in vitro*

The aqueous of AuNRs@MSN and PDA-AuNRs@MSN containing the same Au concentration (20 mg/mL) were added into 0.5 mL centrifuge tube and irradiated by 808 nm laser at a power density of 1 W/cm^2 for 600 s. For the control group, 0.5 mL of deionized water was also irradiated under the same condition. To investigate different concentration of PDA-AuNRs@MSN photothermal effect, the as-prepared PDA-AuNRs@MSN was diluted to different concentrations (Au = 10, 20, 40 and 60 mg/mL) and 0.5 mL sample solution was added into the centrifuge tube and was irradiated by 808 nm laser (1 W/cm^2) for 600 s. For the control group, 0.5 mL of deionized water was also irradiated under the same condition. A thermal imager was used to measure the temperature changes and obtain the infrared thermal images.

In vivo biosafety analysis

Female BALB/c mice (4 weeks) were purchased from SLAC laboratory animal Co, Ltd. (Shanghai) and the animal procedures were complied with the guidelines of the Institutional Animal Care and Use Committee of Tongji University. Female BALB/c mice (4 weeks) were treated by the PDA-AuNRs@MSN (Au = 32 mmol/L) through tail vein injection. The control group was injected with PBS pH 7.4 solution at the same volume. The main organs (heart, liver, spleen, lung, kidney and intestines) were collected after 15 days and were stained with hematoxylin and eosin (H&E) for histological analysis.

In vivo photothermal treatment

4T1 cells (2×10^6 cells in PBS pH 7.4 buffer solution) were injected subcutaneously into the flank of the right fore leg of the female BALB/c mice (4 weeks). When the tumor volume reached 80 mm^3, the mice were randomly divided into 5 groups (n = 3 each group). The mice were treated *via* the tail vein with 100 mL solution of PBS+Laser, DOX+Btz, D/B-PDA-AuNRs@MSN, AuNRs@MSN+Laser, D/B-PDA-AuNRs@MSN+Laser, respectively. After 6 h, the mice were irradiated by 808 nm laser (1 W/cm^2) for 600 s

for laser treating groups. The tumor volume was measured by a digital caliper every 2 days. The tumor volume = length * width^2/2.

In vivo photoacoustic (PA) imaging of tumor

4T1 cells (2×10^6 cells in PBS pH 7.4 buffer solution) were injected subcutaneously into the flank of the right fore leg of the female BALB/c mice (4 weeks). When the tumor volume reached 80 mm^3, the PDA-AuNRs@MSN (Au = 32 mmol/L) was intravenously injected into the mice. The PA imaging of the tumor site at different time points (0, 2 h, 4 h and 6.5 h) were scanned using the Vevo LAZR system. The excitation wavelength was 875 nm.

Characterizations

Transmission electron microscopy (TEM) was conducted on JEM-2100 operating at 200 kV. Zeta potentials were measured on a zeta potential analyzer (Zetasizer Nano ZS90, Malvern). The UV-vis spectrum of the sample was measured with a Cary 50 spectrophotometer (Varian). The surface area, pore size, and pore volume were determined by N_2 adsorption-desorption isotherms obtained at 77 K on a Quantachrome Autosorb-1 (USA). The sample was outgassed at 10^{-3} Torr and 60 ^{0}C for approximately 6 h prior to the adsorption experiment. The PA imaging was conducted on Vevo LAZR system (FujiFilm VisualSonics Inc., America). Fourier Transform Infrared Spectroscopy (FTIR) was measured on a SHIMADZU IR prestige-21 spectrometer. Cell imaging was conducted on TCS SP5 confocal laser scanning microscope (Leica, Germany).

Results And Discussion

Synthesis and characterizations of D/B-PDA-AuNRs@MSN

The synthesis of D/B-PDA-AuNRs@MSN was shown in **Scheme 1**. Firstly, a one-pot seedless-mediated growth method was adopted to synthesize CTAB-stabilized AuNRs. Transmission electron microscopy (TEM) images show that the AuNRs are about 25 nm in length and 8 nm in width (Fig. 1A) and longitudinal surface plasmon resonance (LSPR) peak of 730 nm (Fig. 1D). Then, a mesoporous silica shell layer coating on the surface of the AuNRs by sol-gel method is observed and the thickness of the silica shell is about 20 nm (Fig. 1B). After coating, the LSPR peak was found to shift to 757 nm due to the surface refractive index changes (Fig. 1D). The anticancer drug DOX were loaded into the pores of the AuNRs@MSN by diffusing prior to the PDA deposition. Subsequently, the DOX-AuNRs@MSN were incubated with dopamine hydrochloride in Tris-HCl (pH 8.5, 10 mM) solution to form polydopamine layer. After coating with PDA, a block layer on the surface of the AuNRs@MSN can be observed (Fig. 1C) and the peak of the LSPR has a further red shift to 783 nm (Fig. 1D). The loading of another anticancer drug Btz on the DOX-PDA-AuNRs@MSN was conducted through the conjugation between boronic acid of Btz and catechol of PDA.

Each modification of the AuNRs is confirmed by FT-IR, zeta potential and N_2 absorption-adsorption. FT-IR spectrum of CTAB-AuNRs@MSN shows the characteristic C-H stretching vibrations at 2922 cm^{-1} and 2856 cm^{-1} and C-H deformation vibration around 1480 cm^{-1} [31]. These C-H peaks disappear after removing CTAB. Compared to AuNRs@MSN, PDA-AuNRs@MSN displays an absorption band of 1290 cm^{-1}, which is assigned to the stretching vibration of C-O and primary amine vibration from PDA, which indicates the PDA layer is successfully coated on the surface of the AuNRs@MSN [32] (Fig. 2A). Due to the existence of the CTAB, the AuNRs and CTAB-AuNRs@MSN exhibit a zeta potential of +23.3 mV and +22.2 mV, respectively. After removing the template of CTAB, the potential of AuNRs@MSN has a negative value of -14.5 mV. Moreover, after the AuNRs@MSN are coated with the PDA shell, the potential of the obtained nanoparticles is still -15.0 mV because of the catechol groups on the surface of the PDA-AuNRs@MSN nanoparticles [27, 28, 32] (Fig. 2B). Figure 2C and 2D show the nitrogen adsorption-desorption isotherms, and the pore size distribution diagram of the prepared AuNRs@MSN and PDA-AuNRs@MSN nanoparticles. For the AuNRs@MSN, the BET surface area is 564.76 m^2 g^{-1}, the pore volume is 0.82 cm^3 g^{-1}, and the pore size is about 2.33 nm. After depositing the PDA shell, the BET specific surface area, pore size and the pore volume of the PDA-AuNRs@MSN nanoparticles are smaller than the AuNRs@MSN nanoparticles, and are 62.35 m^2 g^{-1}, 1.89 nm and 0.2 cm^3 g^{-1}, respectively. This further suggests that the PDA shell has been successfully modified on the surface of the AuNRs@MSN nanoparticles.

In vitro drug release

Double anticancer drugs, DOX and Btz, were loaded into the nanoparticles through two different mechanisms. DOX loading was achieved by physical absorption, while Btz was realized by covalent conjugation. The UV-vis spectrum confirms both two anticancer drugs were successfully loaded in the PDA-AuNRs@MSN (Fig. 3). The loading contents of DOX and Btz in PDA-AuNRs@MSN were measured to be 115 mg/g and 6.1 mg/g by calculating the absorbance of the supernatant according to the DOX and Btz standard curve (Fig. 4A-4D). Fig. 4E and 4F show the drug release profiles of DOX and Btz in different pH solutions with or without the laser irradiation. Both anticancer drugs release are pH-dependent. For DOX, the drug release rate is much less at pH 7.4 than that at pH 5.0 because of the PDA layer might be partially peeled from the surface of the nanoparticles at pH 5.0 [27, 28]. For Btz, about 81.7 % of the Btz is released at pH 5.0, while only 18.8 % of the Btz is released at pH 7.4. This difference is attributed to the pH dependence of cleavage of the boronic ester bond.

The drug release rates of DOX and Btz are obviously faster under NIR irradiation at different pH values. The release of Btz from the nanoparticles can be increased to 88.2 % under laser irradiation and acidic condition. This condition can facilitate the cleavage of the boronic ester for drug release [30]. While for the release rate of DOX, it is a slightly increase, which can be ascribed to the heat that accelerates the DOX molecules movement at pH 5.0. These results indicate the release of DOX and Btz are sensitive to pH and heat-dependent.

Photothermal effect of PDA-AuNRs@MSN

In order to prove the deposition of the PDA layer could enhance the photothermal effect, the laser-induced heat generation of PDA-AuNRs@MSN and AuNRs@MSN by 808 nm laser irradiation at a power intensity of 1.0 W cm^{-2} for 10 min were measured under the same Au concentration, respectively. As seen from Fig. 5, the pure water shows little temperature change, which is increased by only 0.2 ^{o}C. The temperature of PDA-AuNRs@MSN is found increased by 31.4 ^{o}C and significantly higher than that of AuNRs@MSN (22.4 ^{o}C) under the same condition. The results demonstrate that the enhanced photothermal effect of the PDA-AuNRs@MSN can be attributed to the PDA shell which increases NIR absorption at 808 nm. Then, we investigated the photothermal effect of different concentrations of PDA-AuNRs@MSN (Au = 10, 20, 40 and 60 mg/mL). We found the temperature increased along with the concentration of the PDA-AuNRs@MSN under the laser continuous irradiation for 10 min.

In vitro cytotoxicity and cell uptake

The cytotoxicity of AuNRs@MSN and PDA-AuNRs@MSN were evaluated by CCK-8 assay. The cell viabilities of the 4T1 cells are over 90% after incubated with AuNRs@MSN and PDA-AuNRs@MSN even at 60 mg/mL of Au concentration, suggesting that the nanoparticles are biocompatibility (Fig. 7A). In order to evaluate the combination therapeutic effect, 4T1 cancer cells were treated with several groups with or without NIR laser irradiation. As shown in Fig. 7B, free D/B treatment shows higher cell cytotoxicity than D/B-PDA-AuNRs@MSN because the drug release is inhibited by the PDA layer. However, upon laser irradiation, D/B-PDA-AuNRs@MSN shows much higher cell killing capability than that of free D/B drugs and AuNRs@MSN. To be specific, PBS+Laser treatment shows very little killing effect on cells due to the low NIR light absorption by endogenous cytochromes. Owing to the enhanced photothermal effect of gold nanorod, ~32.1% of cells were found killed by AuNRs@MSN and ~69.4% of cells were killed by PDA-AuNRs@MSN in the presence of NIR irradiation.

The intracellular uptake of the D/B-PDA-AuNRs@MSN in 4T1 cells was investigated using confocal laser scanning microscopy. After 4 h incubation, red signals were observed in the cell nucleus and cytoplasm, which indicates that the D/B-PDA-AuNRs@MSN could be effectively phagocytized by cells and the loaded DOX could be released from the D/B-PDA-AuNRs@MSN into the cell nucleus (Fig. 7C).

In vivo photoacoustic imaging and photothermal-chemo therapy

Prior to *in vivo* application, we first studied the potential *in vivo* toxicity of the PDA-AuNRs@MSN. HE staining results demonstrate the main organs (heart, liver, spleen, lung, kidney and intestines) have no inflammation or abnormality after 15 days compared with the control group, showing the PDA-AuNRs@MSN could be applied to *in vivo* biomedical application (Fig. 7D).

Due to high NIR absorption, we further investigated the PDA-AuNRs@MSN for *in vivo* PA imaging, which is non-invasive biomedical imaging with high imaging depth and spatial resolution [33]. The optimal photoacoustic excitation wavelength *in vitro* was found to be 875 nm (Fig. 8A) and the PA intensity of the PDA-AuNRs@MSN becomes stronger with the increase of the concentration gradually, and exhibits a certain linear correlation (Fig. 8B). Furthermore, we conducted *in vivo* PA imaging of the PDA-

AuNRs@MSN on 4T1 tumor-bearing mice. As shown in Fig. 8C, a weak PA signal is observed before injecting the PDA-AuNRs@MSN *via* tail vein. The PA signal can be observed in the tumor site at 1.5 h and the intensity is gradually enhanced along with the time, demonstrating the accumulation of PDA-AuNRs@MSN in tumor and could be a good PA imaging contrast agent *in vivo*.

We finally utilized the D/B-PDA-AuNRs@MSN for tumor photothermal-chemo therapy. The 4T1 tumor-bearing mice were randomly divided into five groups: PBS+Laser, DOX+Btz, D/B-PDA-AuNRs@MSN, AuNRs@MSN+Laser and D/B-PDA-AuNRs@MSN+Laser. Upon laser irradiation for 5 min, the tumor temperature rapidly reaches to 61.6 ^{o}C , which would be high enough to kill the tumor cells. In contrast, the tumor temperature treated with AuNRs@MSN and PBS raise by 49.7 ^{o}C and 34.0 ^{o}C, respectively (Fig. 9A). Compared to the AuNRs@MSN group, the tumor growth of the D/B-PDA-AuNRs@MSN is significantly inhibited after irradiation (Fig. 9B). It should be noted that PBS+laser has no treatment effect on tumor since the laser power is controlled at the safety range. Free drugs are rapidly metabolized *in vivo*. The D/B-PDA-AuNRs@MSN can be accumulated in the tumor site through the enhanced permeability and retention (EPR) effect, thus the inhibitory effect of D/B-PDA-AuNRs@MSN on tumor is better than D/B alone. Meanwhile, no obvious body weight loss in the whole treatment period (Fig. 9C).

The tumor of each group was stripped for HE analysis to evaluate the therapeutic efficiency after the treatment period. The D/B-PDA-AuNRs@MSN group shows significant cancer cell damage than either photothermal therapy or chemotherapy alone (Fig. 9D). Taken together, the D/B-PDA-AuNRs@MSN could serve as a theranostic probe for tumor imaging-guided therapy.

Conclusions

In summary, we designed a multifunctional drug delivery system based on D/B-PDA-AuNRs@MSN for tumor PA imaging-guided chemo-photothermal therapy, which combines double drug loading and pH/thermal dual responsive drug release. The presence of the PDA layer not only loads the anticancer drug and controls the drug release, but also enhances the photothermal effect. The *in vitro* and *in vivo* experiments show D/B-PDA-AuNRs@MSN can be effectively internalized by the cancer cells and particularly it exerts high-quality PA imaging-guided chemo and photothermal therapies in tumor. Thus, the developed multifunctional D/B-PDA-AuNRs@MSN theranostic probe could serve as an effective probe for the treatment of cancers.

Declarations

Authors' contributions

WJ-the experimental design and manuscript preparation. WJ and CN-in vitro and in vivo experiment, WJ, LK and ZW-the synthesis and characterization of nanoparticles. WJ and CN contributed equally to this work and should be considered as co-first authors. YW, TY, GX and ZB-manuscript preparation and review. All authors read and approved the final manuscript.

Author details

[1] Department of Medical Ultrasound, Shanghai Tenth People's Hospital, Tongji University Cancer Center, Tongji University School of Medicine, Shanghai 200072, China. [2] State Key Laboratory of Radiation Medicine and Protection, School of Radiation Medicine and Protection, Collaborative Innovation Center of Radiological Medicine of Jiangsu Higher Education Institutions, Soochow University, Suzhou 215123, China. [3] Department of Radiology, Luodian Hospital, Baoshan Branch of Fudan University Shanghai Cancer Center, Shanghai 201908, China.

Corresponding author: bingbozhang@tongji.edu.cn

tuyu@suda.edu.cn

gao_xiaolong@tongji.edu.cn

Availability of Data and Materials

All data generated or analyzed during this study are included in this article.

Acknowledgements

Not applicable.

Conflicts of interests

There are no conflicts to declare.

Consent of publication

Not applicable.

Ethics approval and consent to participate

All animal experiments were approved by the guidelines of the Institutional Animal Care and Use Committee of Tongji University.

Funding

We gratefully acknowledge the financial support from the National Natural Science Foundation of China (Grant No. 81571742, 81871399, 81922035, 81801823), and Shanghai Science and Technology Biomedical Innovation Funds (Grant No. 19441904200).

Abbreviations

PDA-AuNRs@MSN: polydopamine-coated mesoporous silica-gold nanorods; DOX: doxorubicin; Btz: bortezomib; NIR: near-infrared; PTT: photothermal therapy; AuNPs: gold nanoparticles ; AuNCs: gold nanocages; LSPR: longitudinal surface plasmon resonance; PDA: polydopamine; TEOS: tetraethylorthosilicate; CTAB: cetyltrimethylammonium bromide; DMSO: dimethylsulfoxide; LE: loading efficiency; PA: photoacoustic; FTIR: fourier transform infrared spectroscopy; TEM: transmission electron microscopy; AA: ascorbic acid; DAPI: 4, 6-diamidino-2-phenylindole; $AgNO_3$: silver nitrate; $NaBH_4$: sodium borohydride; $HAuCl_4{\cdot}3H_2O$: Tetrachloroauric acid; DOX·HCl: Doxorubicin hydrochloride.

References

1. A R David, M R Zimmerman. Cancer: An old disease, a new disease or something in between? Nat Rev Cancer. 2010;10:728-733.
2. L Cheng, C Wang, L Feng, K Yang and Z Liu. Functional nanomaterials for phototherapies of cancer. Chem Rev. 2014;114:10869-10939.
3. D Zhang, T Wu, X Qin, Q Qiao, L Shang, Q Song, C Yang and Z Zhang. Intracellularly generated immunological gold nanoparticles for combinatorial photothermal therapy and immunotherapy against tumor. Nano Lett. 2019, DOI: 10.1021/acs.nanolett.9b02903.
4. T Liu, R Jin, P Yuan, Y Bai, B Cai and X Chen. Intracellular enzyme-triggered assembly of amino acid-modified gold nanoparticles for accurate cancer therapy with multimode. ACS Appl Mater Interfaces. 2019;11:28621-28630.
5. E Higbee-Dempsey, A Amirshaghaghi, M J Case, J Miller, T M Busch and A Tsourkas. Indocyanine green–coated gold nanoclusters for photoacoustic imaging and photothermal therapy. Adv Therapeutics. 2019;0:1900088.
6. Y-T Liao, C-H Liu, Y Chin, S-Y Chen, S H Liu, Y-C Hsu and K C W Wu. Biocompatible and multifunctional gold nanorods for effective photothermal therapy of oral squamous cell carcinoma. J Mater Chem B. 2019;7:4451-4460.
7. W Sun, K Ge, Y Jin, Y Han, H Zhang, G Zhou, X Yang, D Liu, H Liu, X-J Liang and J Zhang. Bone-targeted nanoplatform combining zoledronate and photothermal therapy to treat breast cancer bone metastasis. ACS Nano. 2019;13:7556-7567.
8. D Liu, W Li, X Jiang, S Bai, J Liu, X Liu, Y Shi, Z Kuai, W Kong, R Gao and Y Shan. Using near-infrared enhanced thermozyme and scfv dual-conjugated au nanorods for detection and targeted photothermal treatment of alzheimer's disease. Theranostics. 2019;9:2268-2281.
9. T Ye, Y Lai, Z Wang, X Zhang, G Meng, L Zhou, Y Zhang, Z Zhou, J Deng, M Wang, Y Wang, Q Zhang, X Zhou, L Yu, H Jiang and X Xiao. Precise modulation of gold nanorods for protecting against malignant ventricular arrhythmias via near-infrared neuromodulation. Adv Funct Mater. 2019;0:1902128.
10. Y Feng, Y Cheng, Y Chang, H Jian, R Zheng, X Wu, K Xu, L Wang, X Ma, X Li and H Zhang. Time-staggered delivery of erlotinib and doxorubicin by gold nanocages with two smart polymers for

reprogrammable release and synergistic with photothermal therapy. Biomaterials. 2019;217:119327.

11. Z Qin, T Du, Y Zheng, P Luo, J Zhang, M Xie, Y Zhang, Y Du, L Yin, D Cui, Q Lu, M Lu, X Wang and H Jiang. Glutathione induced transformation of partially hollow gold–silver nanocages for cancer diagnosis and photothermal therapy. Small. 2019;0:1902755.
12. C Zhan, Y Huang, G Lin, S Huang, F Zeng and S Wu. A gold nanocage/cluster hybrid structure for whole-body multispectral optoacoustic tomography imaging, egfr inhibitor delivery, and photothermal therapy. Small. 2019;0:1900309.
13. F Xia, J Niu, Y Hong, C Li, W Cao, L Wang, W Hou, Y Liu and D Cui. Matrix metallopeptidase 2 targeted delivery of gold nanostars decorated with IR-780 iodide for dual-modal imaging and enhanced photothermal/photodynamic therapy. Acta Biomater. 2019;89:289-299.
14. F Hou, Y Zhu, Q Zou, C Zhang, H Wang, Y Liao, Q Wang, X Yang and Y Yang. One-step preparation of multifunctional alginate microspheres loaded with in situ-formed gold nanostars as a photothermal agent. Mater Chem Frontiers. 2019, DOI: 10.1039/C9QM00276F.
15. C Song, F Li, X Guo, W Chen, C Dong, J Zhang, J Zhang and L Wang. Gold nanostars for cancer cell-targeted SERS-imaging and NIR light-triggered plasmonic photothermal therapy (PPTT) in the first and second biological windows. J Mater Chem B. 2019;7:2001-2008.
16. M Valeria De, C Mariafrancesca, T Chiara Cristina and R Rosaria. Engineered gold nanoshells killing tumor cells: New perspectives. Curr Pharm Des. 2019;25:1-13.
17. X Zhang, Y Liu, L Luo, L Li, S Xing, T Yin, K Bian, R Zhu and D Gao. A chemo-photothermal synergetic antitumor drug delivery system: Gold nanoshell coated wedelolactone liposome. Mater Sci Eng C. 2019;101:505-512.
18. S Yang, Q You, L Yang, P Li, Q Lu, S Wang, F Tan, Y Ji and N Li. Rodlike MSN@Au nanohybrid-modified supermolecular photosensitizer for NIRF/MSOT/CT/MR quadmodal imaging-guided photothermal/photodynamic cancer therapy. ACS Appl Mater Interfaces. 2019;11:6777-6788.
19. S Lu, X Li, J Zhang, C Peng, M Shen and X Shi. Dendrimer-stabilized gold nanoflowers embedded with ultrasmall iron oxide nanoparticles for multimode imaging–guided combination therapy of tumors. Adv Sci. 2018;5:1801612.
20. Y Zhang, T-T Shen, H-L Zhang, A M Kirillov, H-J Cai, J Wu, W-S Liu and Y Tang. A multifunctional nanocomposite for luminescence resonance energy transfer-guided synergistic monitoring and therapy under single near infrared light. Chem Commun. 2016;52:4880-4883.
21. L Zhang, H Su, J Cai, D Cheng, Y Ma, J Zhang, C Zhou, S Liu, H Shi, Y Zhang and C Zhang. A multifunctional platform for tumor angiogenesis-targeted chemo-thermal therapy using polydopamine-coated gold nanorods. ACS Nano. 2016;10:10404-10417.
22. Y-T Chang, P-Y Liao, H-S Sheu, Y-J Tseng, F-Y Cheng and C-S Yeh. Near-infrared light-responsive intracellular drug and sirna release using au nanoensembles with oligonucleotide-capped silica shell. Adv Mater. 2012;24:3309-3314.
23. Z Zhang, L Wang, J Wang, X Jiang, X Li, Z Hu, Y Ji, X Wu and C Chen. Mesoporous silica-coated gold nanorods as a light-mediated multifunctional theranostic platform for cancer treatment. Adv Mater.

2012;24:1418-1423.

24. J Song, X Yang, O Jacobson, P Huang, X Sun, L Lin, X Yan, G Niu, Q Ma and X Chen. Ultrasmall gold nanorod vesicles with enhanced tumor accumulation and fast excretion from the body for cancer therapy. Adv Mater. 2015;27:4910-4917.
25. J Song, X Yang, O Jacobson, L Lin, P Huang, G Niu, Q Ma and X Chen. Sequential drug release and enhanced photothermal and photoacoustic effect of hybrid reduced graphene oxide-loaded ultrasmall gold nanorod vesicles for cancer therapy. ACS Nano. 2015;9:9199-9209.
26. I Gorelikov and N Matsuura. Single-step coating of mesoporous silica on cetyltrimethyl ammonium bromide-capped nanoparticles. Nano Lett. 2008;8:369-373.
27. D Chang, Y Gao, L Wang, G Liu, Y Chen, T Wang, W Tao, L Mei, L Huang and X Zeng. Polydopamine-based surface modification of mesoporous silica nanoparticles as ph-sensitive drug delivery vehicles for cancer therapy. J Coll Interface Sci. 2016;463:279-287.
28. Q Zheng, T Lin, H Wu, L Guo, P Ye, Y Hao, Q Guo, J Jiang, F Fu and G Chen. Mussel-inspired polydopamine coated mesoporous silica nanoparticles as ph-sensitive nanocarriers for controlled release. Inter J Pharm. 2014;463:22-26.
29. A R K Sasikala, A GhavamiNejad, A R Unnithan, R G Thomas, M Moon, Y Y Jeong, C H Park and C S Kim. A smart magnetic nanoplatform for synergistic anticancer therapy: Manoeuvring mussel-inspired functional magnetic nanoparticles for ph responsive anticancer drug delivery and hyperthermia. Nanoscale. 2015;7:18119-18128.
30. R Zhang, S Su, K Hu, L Shao, X Deng, W Sheng and Y Wu. Smart micelle@polydopamine core-shell nanoparticles for highly effective chemo-photothermal combination therapy. Nanoscale. 2015;7:19722-19731.
31. J Wang, H Liu, F Leng, L Zheng, J Yang, W Wang and C Z Huang. Autofluorescent and ph-responsive mesoporous silica for cancer-targeted and controlled drug release. Microp Mesop Mater. 2014;186:187-193.
32. R Zheng, S Wang, Y Tian, X Jiang, D Fu, S Shen and W Yang. Polydopamine-coated magnetic composite particles with an enhanced photothermal effect. ACS Appl Mater Interfaces. 2015;7:15876-15884.
33. G Ku, M Zhou, S Song, Q Huang, J Hazle and C Li. Copper sulfide nanoparticles as a new class of photoacoustic contrast agent for deep tissue imaging at 1064 nm. ACS Nano. 2012;6:7489-7496.

Figures

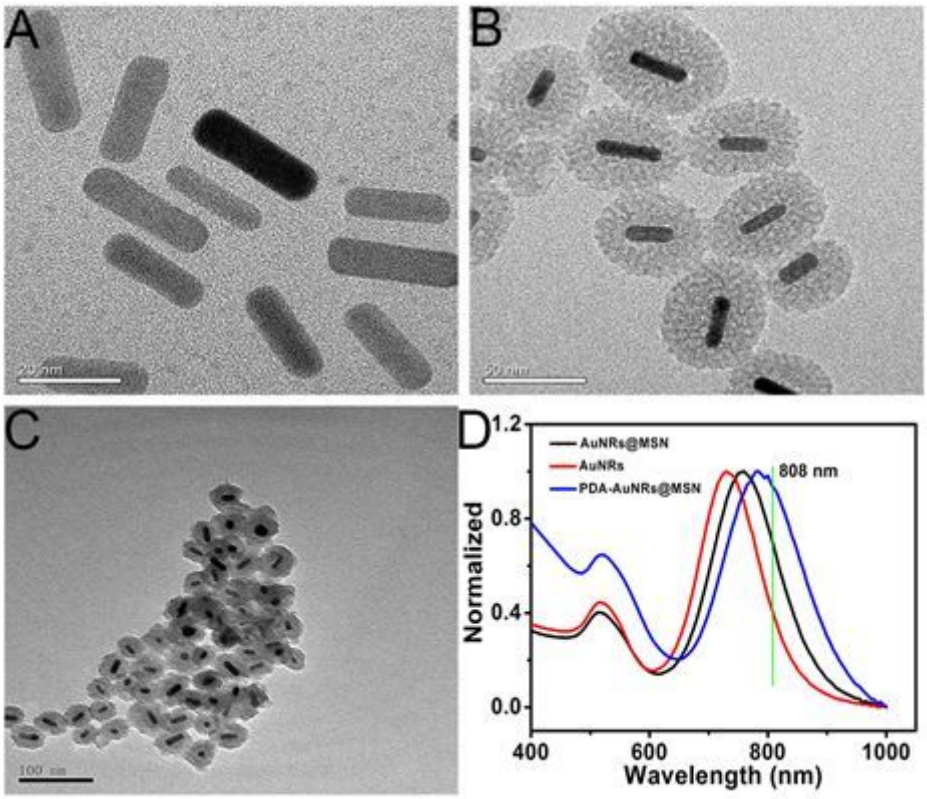

Figure 1

The TEM images of the AuNRs (A), AuNRs@MSN (B) and PDA-AuNRs@MSN (C); the UV-vis spectrum of the AuNRs, AuNRs@MSN and PDA-AuNRs@MSN (D).

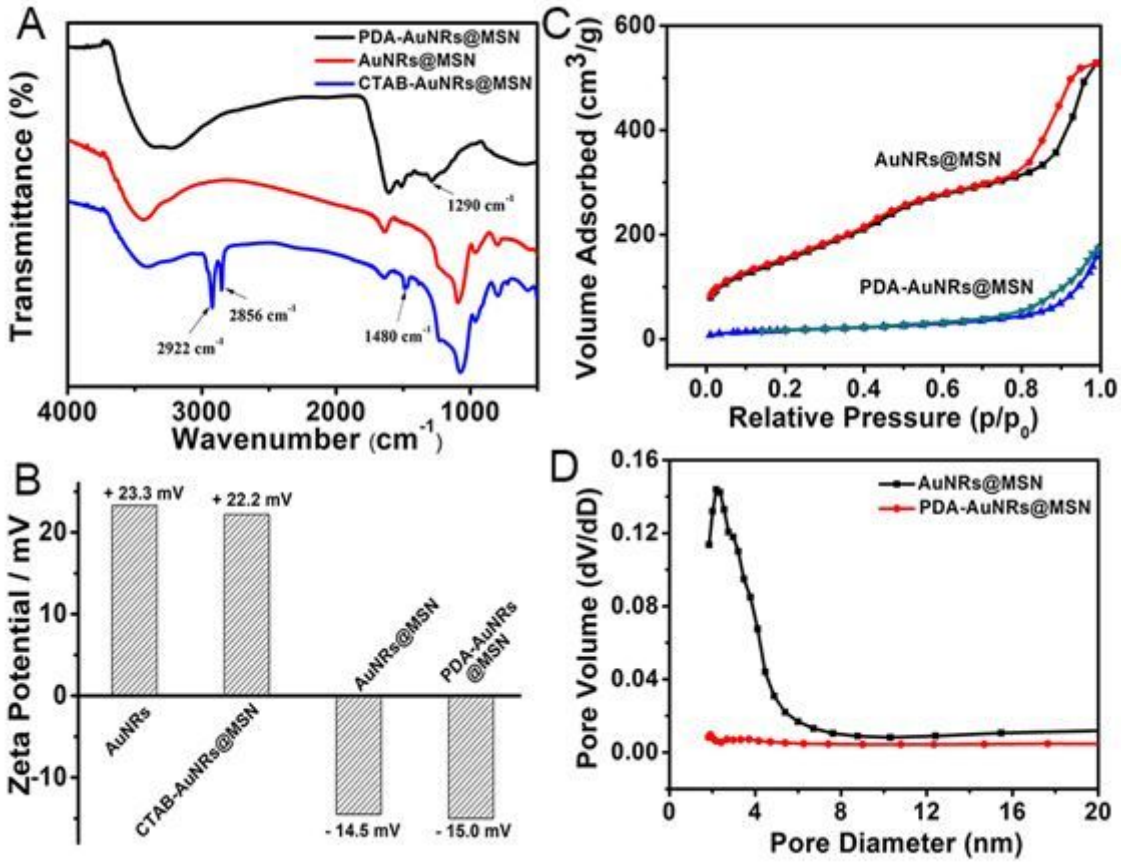

Figure 2

FT-IR spectra of CTAB-AuNRs@MSN, AuNRs@MSN and PDA-AuNRs@MSN. (A), Zeta potentials (B), Nitrogen adsorption-desorption isotherms (C) and pore size distributions (D) of the as-synthesized AuNRs@MSN and PDA-AuNRs@MSN.

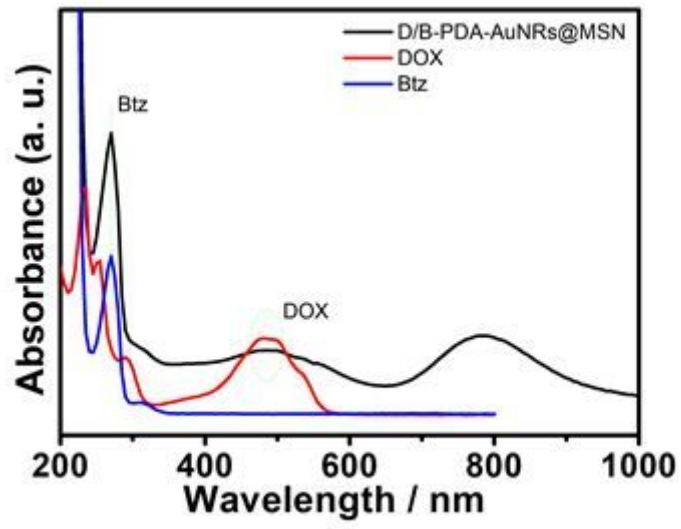

Figure 3

The UV-vis spectra of the DOX, Btz and D/B-PDA-AuNRs@MSN

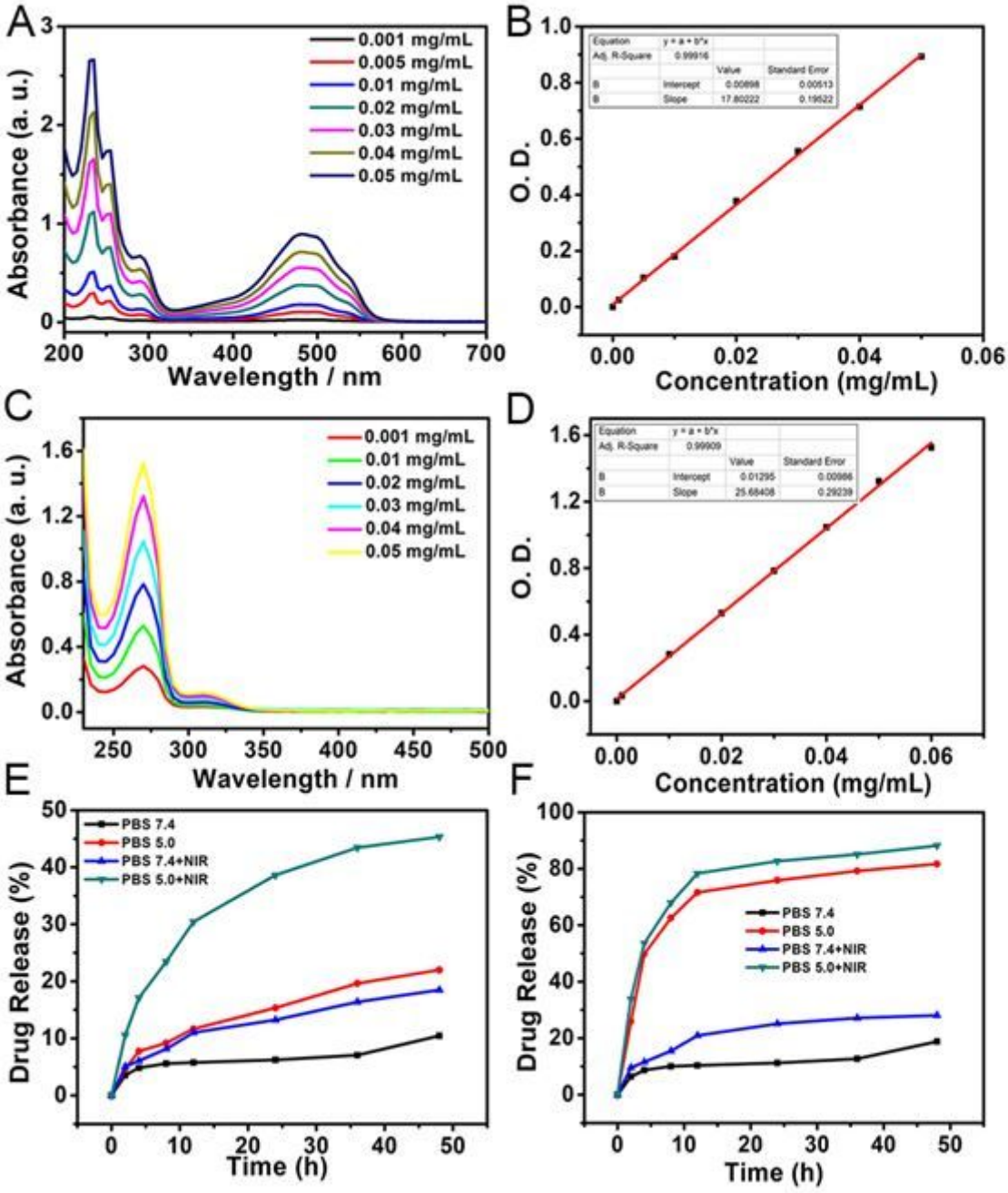

Figure 4

The standard curve of concentration-dependent DOX absorbance at 480 nm in water (A, B); the standard curve of concentration-dependent Btz absorbance at 270 nm in water (C, D); cumulative drug release profiles of the DOX (E) and Btz (F) from D/B-PDA-AuNRs@MSN in PBS at pH values of 7.4 and 5.0 with or without NIR irradiation, respectively.

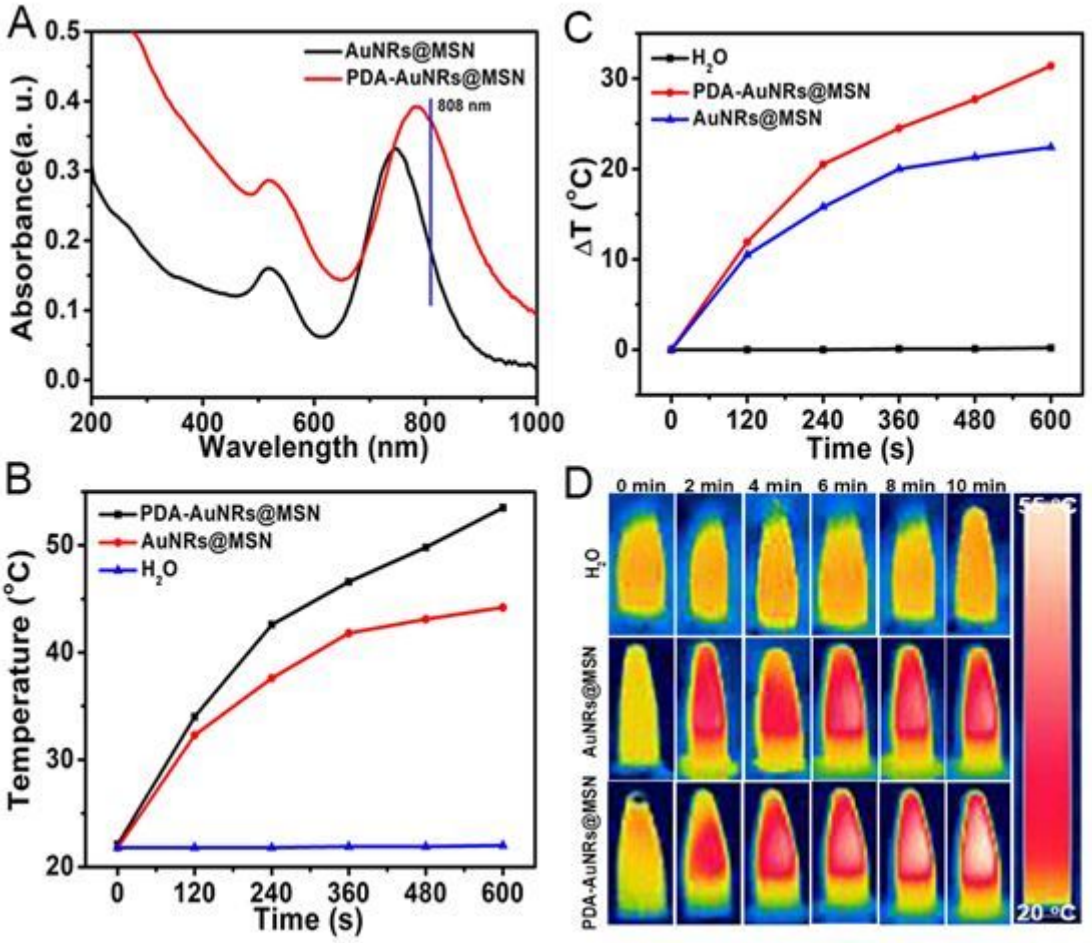

Figure 5

The UV−vis absorption spectra of PDA-AuNRs@MSN and AuNRs@MSN aqueous solution at the same Au concentration (20 □g/mL) (A); Temperature elevation of PDA-AuNRs@MSN and AuNRs@MSN under NIR laser irradiation (808 nm, 1 W/cm2, 10 min) (B); temperature changes versus PDA-AuNRs@MSN and AuNRs@MSN (C); The infrared thermal images of PDA-AuNRs@MSN and AuNRs@MSN at the same different Au concentration under NIR laser irradiation (808 nm, 1 W/cm2, 10 min) (D).

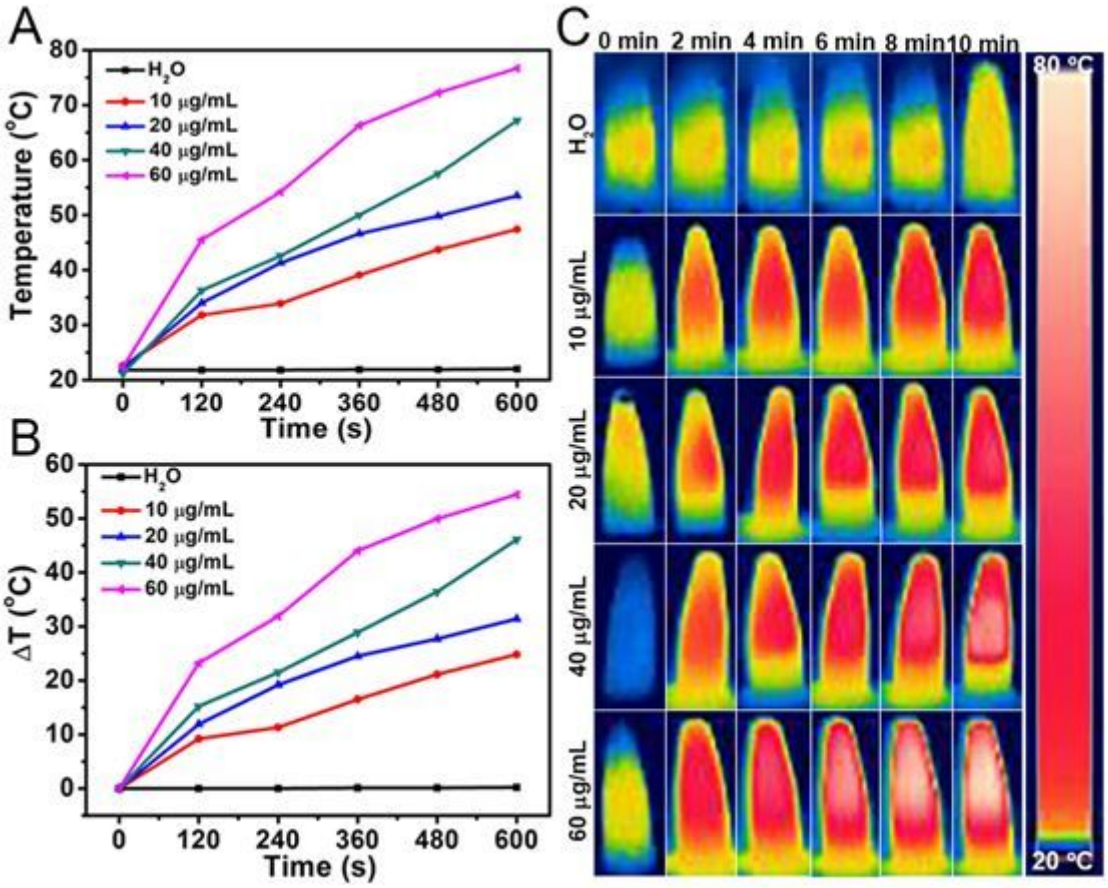

Figure 6

Temperature elevation of PDA-AuNRs@MSN aqueous solution at different Au concentration under NIR laser irradiation (808 nm, 1 W/cm2, 10 min) (A); temperature changes versus the different Au concentration of PDA-AuNRs@MSN (B); The infrared thermal images of PDA-AuNRs@MSN at different Au concentration under NIR laser irradiation (808 nm, 1 W/cm2, 10 min) (C).

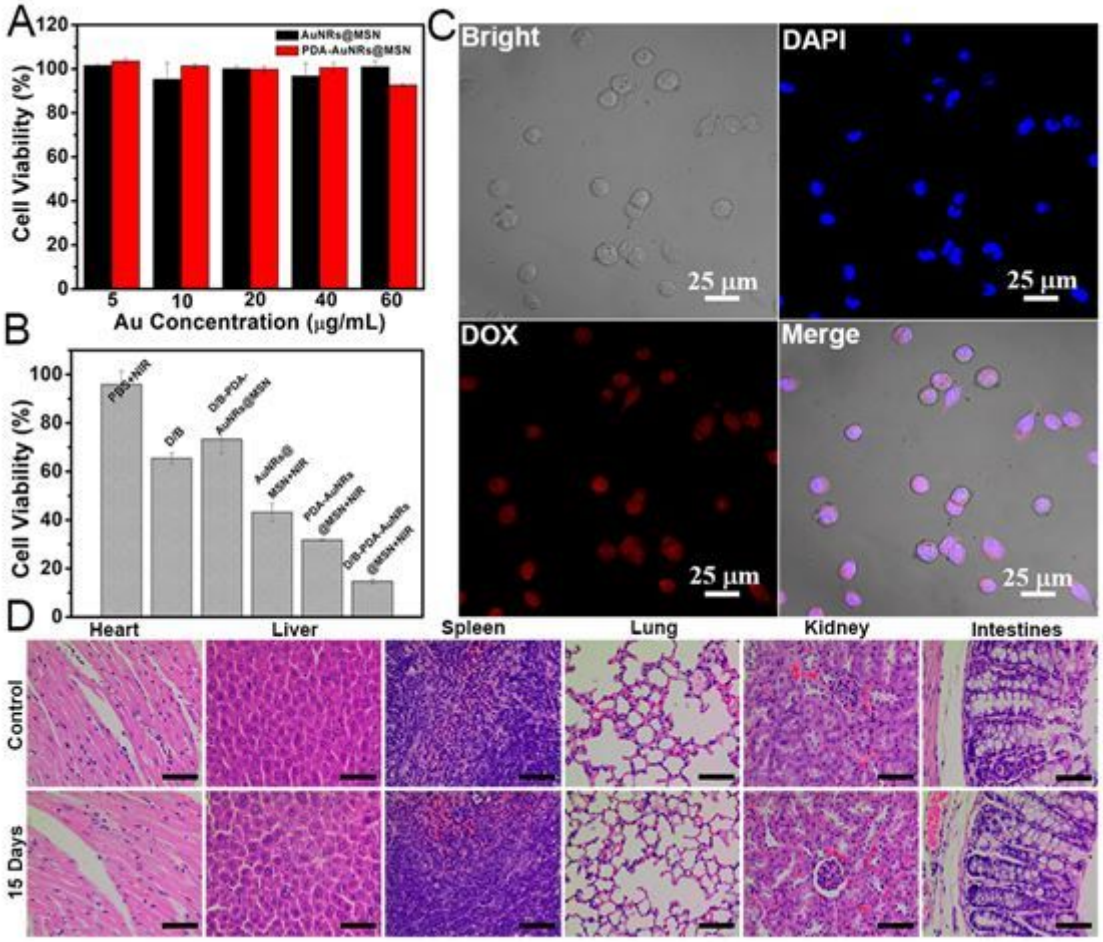

Figure 7

The cell viabilities of the 4T1 cells treated with AuNRs@MSN and PDA-AuNRs@MSN at different concentrations for 24 h (A); The cell viabilities of 4T1 cells treated with PBS (a), free DOX/Btz (D/B) (b), D/B-PDA-AuNRs@MSN (c), AuNRs@MSN+NIR (d), PDA-AuNRs@MSN+NIR (e) and D/B-PDA-AuNRs@MSN+NIR (f) with laser irradiation for 5 min at 37 oC for 24 h (DOX concentration: 2 □g/mL, Btz concentration: 0.1 □g/mL) (B); The confocal microscopic images of 4T1 cells incubated with D/B-PDA-AuNRs@MSN for 4 h at 37 °C (DOX concentration = 2 μg/mL). The nuclei was stained by DAPI (C); H&E-staining images of major organs (heart, liver, spleen, lung, kidney and intestines) of the mice collected from the blank mice and the 15 days after intravenous injection of PDA-AuNRs@MSN (Au concentration: 32 mmol/L). Scale bar is 20 μm (D).

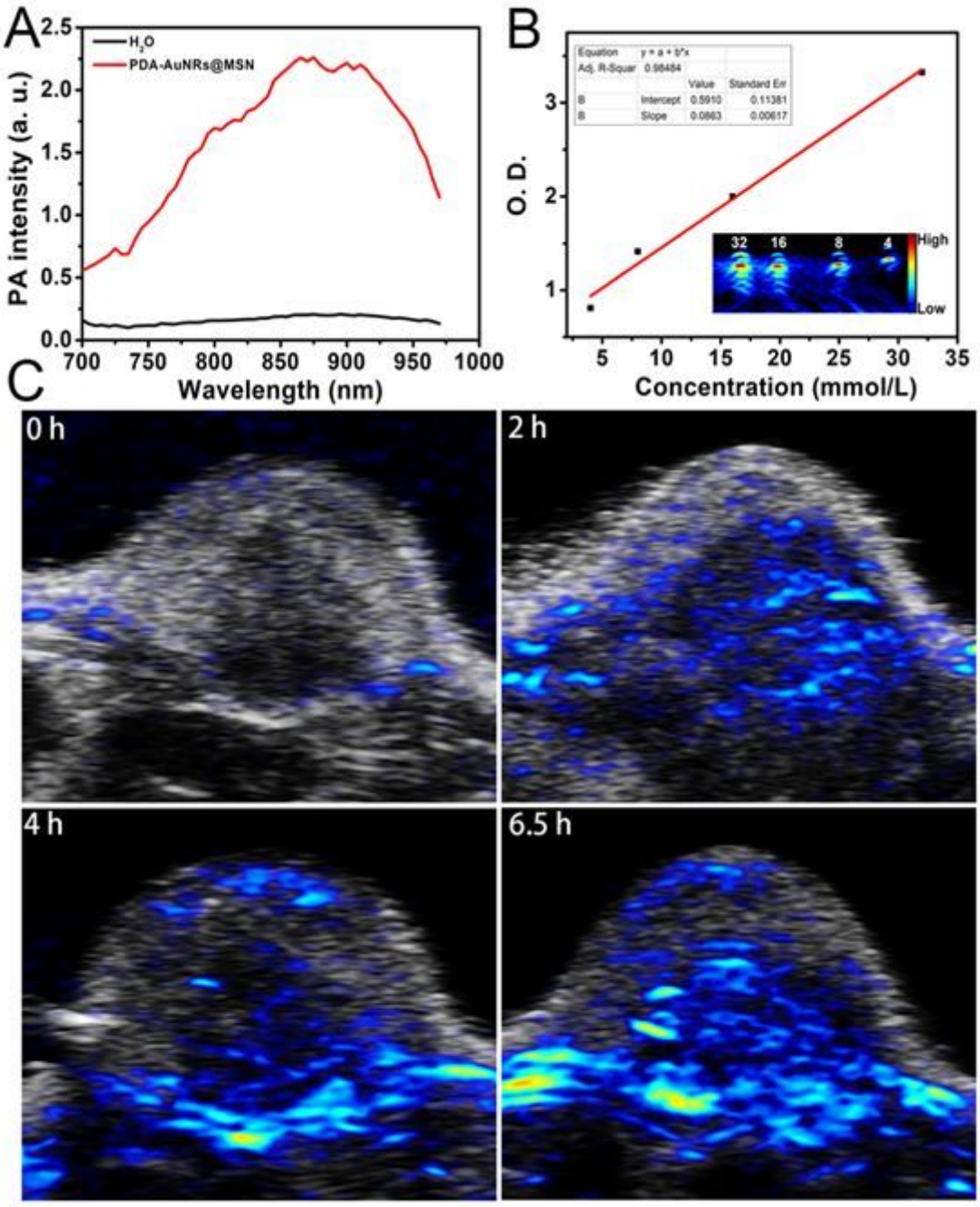

Figure 8

Determination of the optimal excitation wavelength of photoacoustic imaging (A); the linear relationship between PA signal intensity and concentration of PDA-AuNRs@MSN. Inset: PA imaging phantoms (B); In vivo photoacoustic images of the 4T1-tumor-bearing mouse with intravenous injection of PDA-AuNRs@MSN at different time points (C).

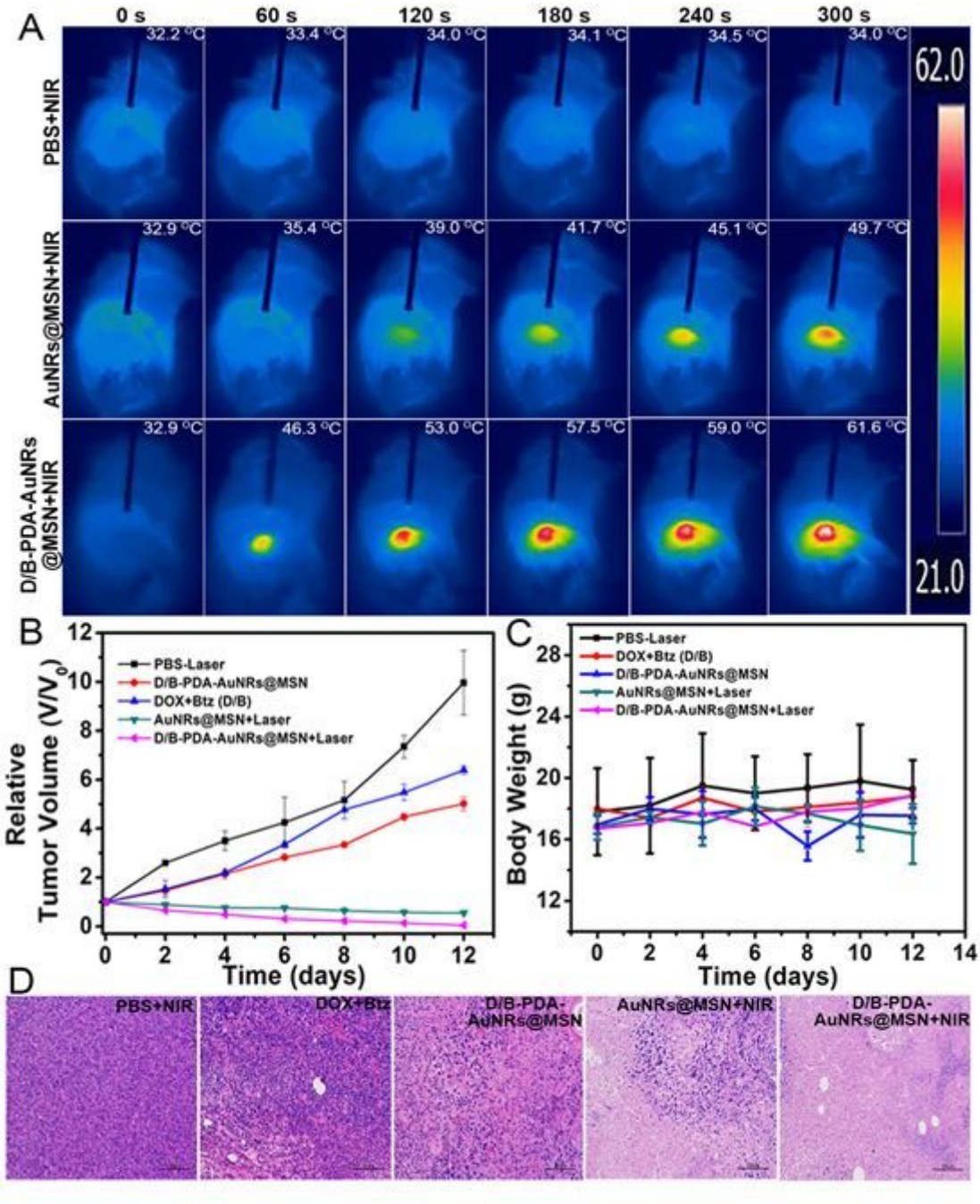

Figure 9

The infrared thermal images of 4T1-tumor-bearing mice with intravenous injection of PBS (200 □L), AuNRs@MSN (200 □L, 32 mmol/L) and D/B-PDA-AuNRs@MSN (200 □L, 32 mmol/L) and then irradiated with an 808 nm NIR laser (1.0 W/cm2) for 5 min (A). Tumor growth (B) and body weight (C) curves after different treatments; HE staining of tumor tissues from various treatment groups (D). Scale bar is 100 μm.

Supplementary Files

This is a list of supplementary files associated with this preprint. Click to download.

- scheme1.JPG